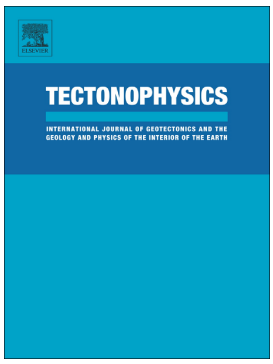

Extensional vs. compressional deformation in the Central High Atlas salt province: A paleomagnetic approach

P. Calvín, A.M. Casas-Sainz, J.J. Villalaín, B. Moussaid

PII: S0040-1951(18)30140-9
DOI: doi:10.1016/j.tecto.2018.04.007
Reference: TECTO 127819

To appear in: *Tectonophysics*

Received date: 6 July 2017
Revised date: 3 April 2018
Accepted date: 6 April 2018

Please cite this article as: P. Calvín, A.M. Casas-Sainz, J.J. Villalaín, B. Moussaid , Extensional vs. compressional deformation in the Central High Atlas salt province: A paleomagnetic approach. The address for the corresponding author was captured as affiliation for all authors. Please check if appropriate. Tecto(2017), doi:10.1016/j.tecto.2018.04.007

Extensional vs. compressional deformation in the Central High Atlas salt province: a paleomagnetic approach

P. Calvín[1,*], A. M. Casas-Sainz[2], J. J. Villalaín[1], and B. Moussaid[3]

[1]Laboratorio de Paleomagnetismo, Universidad de Burgos, Spain.

[2]Geotransfer Research Group (IUCA), Universidad de Zaragoza, Spain.

[3]Laboratoire BGIM, Ecole Normale Supérieure, Université Hassan II. Casablanca, Morocco.

[*]Corresponding author: Pablo Calvín (calvinballester@gmail.es). Dep. Física, Escuela Politécnica Superior, Río Vena, Universidad de Burgos, Av. Cantabria s/n, 09006 Burgos, Spain.

Abstract

In this paper we address the problem of the distinction between diapiric, salt-driven and compressional structures, using the outstanding example of the Central High Atlas (Morocco). A remagnetized component carried by magnetite has been isolated in 32 new paleomagnetic sites. It is characterized by: maximum unblocking temperatures around 450ºC, syn-folding behavior and normal polarity.

These 33 mean paleomagnetic directions were analyzed together with other 68 from published works around the study area to construct a robust paleomagnetic dataset along a cross-section perpendicular to the main structures. The remagnetization direction (n: 100, Dec: 332.2º, Inc: 34.5º, η: 6.2º, ξ: 2.0º, A/n: 6.427º) and the paleo-dip of beds (the attitude of the beds at the remagnetization occurrence) were calculated through small circle methods. The remagnetization can

be dated as *ca*. 100 Ma. Because of its occurrence between the extensional and compressional periods, this remagnetization offers the possibility of restore the basin to its pre-inversion geometry.

Comparison between present-day and pre-inversion structure allows discriminating three different evolutionary patterns: (i) thrusted and welded salt-walls mainly structured during the extensional stage (Ikkou ridge) with steep limbs close to the salt-wall core. (ii) Jurassic salt-walls with weaker deformation, restricted to the areas adjacent to the structure (Tadaghmamt and Timedouine); in this case, Cenozoic compression is limited to welding of the salt-walls and buttressing of the sedimentary sequences against faults. (iii) salt-rollers gently initiated during the Jurassic (Toumliline diapir), thrusted during the Cenozoic compression. Results show the importance of salt tectonics both during extension and compression, as well as the control of the compressional features by the inherited extensional structures. The performed restorations prove that paleomagnetism is a useful, independent tool to obtain palinspastic restorations and to separate, and quantify, the imprint generated during the basinal stage from the inversional features.

Key words: Chemical remagnetization; Central High Atlas; Small Circle methods; salt-wall; diapir; paleomagnetic restoration.

1. Introduction

Halokinetic processes are one of the main deformation mechanisms in inverted basins having basal or intermediate thick salt layers. Diapir-related structures (salt-walls, diapirs, salt-cored anticlines, etc.) can develop either associated with extension during the basinal stage (e.g. Vendeville and Jackson, 1992; Ferrer et al., 2012; Jackson and Lewis, 2016) or with compression during subsequent basin inversion (Davis and Engelder, 1985; Costa and Vendeville, 2002; Santolaria et al., 2015). The triggering mechanism is commonly differential loading, easily

generated as a consequence of extensional or compressional activity. At the same time, presence of salt levels and related halokinetic processes interact with regional tectonism, controlling basic aspects such as subsidence the location of depocenters (Jackson and Lewis, 2016, and references therein), or the style of folding or thrusting in the case of compression (e.g. Davis and Engelder, 1985). Furthermore, structures generated during extension are usually reactivated and squeezed during inversion and therefore their present-day geometry is a consequence of the contribution from both stages. The study of the geometry of strata adjacent to salt-bodies gives clues about the relationships between tectonic, halokinetic and sedimentation processes (e.g. Giles and Lawton, 2002). However, quantifying the deformation related to extension or compression is not straightforward and chronological constrains, provided that they are reliably placed within the frame of geological events, are necessary to address this issue.

Paleomagnetic works applied to diapirs are scarce, but they have been successful in unraveling different topics regarding diapir emplacement and evolution. A pioneering work in this sense was carried by Weinberger et al. (1997) who distinguished two main stages of evolution of the Sedom Diapir (Dead Sea Rift). Henry et al. (2000) and Roca et al. (2013) shed light in the evolution of Triassic diapiric bodies in Tunisia and the Prebetic Zone (SE Spain), respectively, allowing to substantiate emplacement hypotheses. Finally, Torres-López et al. (2016) separated in the Central High Atlas (CHA) the Jurassic deformation directly caused by salt tectonics and igneous intrusions from the deformation due to the Cenozoic compression.

The exceptional outcrops of the CHA have been exploited in the development of several research works focused on the tectono-stratigraphic relationships in extensional setting in which halokinetic activity plays a major role (Bouchouata et al., 1995; Ettaki et al, 2007; Michard et al., 2011; Saura et al., 2014; Joussiane, 2016; Malaval, 2016; Martín-Martín et al., 2017; Teixell et al., 2017; Vergés et al., 2017). These works evidence the presence of an intense halokinetic activity during the Early and Middle Jurassic that, together with the activity of the extensional faults, controlled the

sedimentation through ENE-WSW trending salt-walls (called ‘ridges’ in the literature), that limited sedimentary depocenters. During the subsequent Cenozoic inversion of the basin (Mattauer et al., 1977; Michard et al., 1976), these structures were squeezed, modifying their syn-extensional original geometry (Teixell et al., 2017; Vergés et al., 2017).

Nevertheless, the contribution of extensional (or diapiric) and compressional deformation to the final development of structures is still unknown. We even ignore whether similar structures have the same or different origins. The main objective of this paper is focused on deciphering the origin of structures by means of the quantification of their chronological development by means of paleomagnetic tools. We use the *ca*. 100 Ma remagnetization found in the CHA (Torres-López et al. 2014), which separates the basinal and the inversional stages, to quantify the deformation related to each process. We demonstrate that compressional features, and specially fold separation and wavelength, are beyond the laws of buckling (e.g. Fletcher, 1974; Kocher et al., 2006) and that other constraints, namely inherited heterogeneities and previous, diapiric folding are key in the process of fold growth. Consequently, folds formerly considered as compressional must be explained by growth during prevailing extensional tectonic regimes. In this way, paleomagnetism has revealed itself as a powerful to approach, from a quantitative point of view, to the original geometry resulting from the basinal stage and the subsequent development of folding during basin inversion.

2. Geological framework

The Atlas system is a set of intracontinental chains (Mattauer et al., 1977) located in the southwestern foreland of the Mediterranean Alpine System (Fig. 1). It extends from the Atlantic coast of Morocco to the Mediterranean coast of Tunisia, conforming a 100 km wide, 2000 km long

mountain belt. The Atlas is the result of the tectonic inversion during the Cenozoic of extensional Mesozoic basins, due to the convergence between African and European plates (e.g. Mattauer et al., 1977; Gomez et al., 2000). The Central High Atlas (CHA) is located in the mid-western sector of the mountain chain and is characterized by thick Lower-Middle Jurassic sedimentary sequences, folded according to long, tight ENE-WSW anticlines that limit open, gentle synclines (Fig. 2).

A synthesis of the Mesozoic evolution of the CHA can be found in Frizon de Lamotte et al., (2008). Summarizing, this evolution shows a first rifting event during the Triassic (Fig. 1c), characterized by deposit of red beds which crop out towards the western part of the chain, in the Marrakech High Atlas (e.g. Domènech et al., 2015), and evaporites and shales to the top of the sequence, capped by basaltic rocks related to the CAMP event (e.g. Knight et al., 2004). Shales and salts are the regional décollement for many tectonic structures. It played a major role during the Mesozoic extension (and dominant in diapiric processes) and during the Cenozoic inversion (as the basal detachment that favors the decoupling between the basement and the cover) as well.

During the Early Jurassic, a new, intense rift stage took place, resulting in the deposit of thick sedimentary sequences: more than 5000 m of Jurassic rocks accumulated in the depocenters until the end of Bajocian times (Frizon de Lamotte et al., 2008, and references therein). During this stage, diapiric processes also played an important role in the configuration of the basin (Ettaki et al., 2007; Michard et al., 2011), partly controlling the subsidence rate and localization of depocenters (Moragas et al., 2016), that were bounded by large salt-walls (Saura et al., 2014). The NE-SW to ENE-WSW trend of these structures is strongly conditioned by basement faults (Mattauer et al., 1977; Schaer, 1987; Charrière, 1990), what suggest that normal faulting was one of the main factors triggering halokinetic activity.

At the end of this extensional stage, a new alkaline to transitional magmatic event took place. It was characterized in the study area by mafic intrusions (mainly gabbros) dated as Upper Jurassic (Hailwood and Mitchell, 1971; Armando, 1999). These rocks crop out at the core of the

anticlines, mixed in different proportions (in each particular structure) with Triassic rocks (Calvín et al., 2017a).

Absence of Upper Jurassic-Lower Cretaceous sedimentary rocks limit the precise bracketing of the evolution of the CHA during this time, and a general uplift during the Late Jurassic has been invoked (Laville and Piqué, 1992; Beauchamp et al., 1999; Frizon de Lamotte et al., 2008). However, a compressional uplift is in disagreement both with the fission tracks paths (Barbero et al., 2007) and with the *ca*. 100 Ma widespread remagnetization (see next section for discussion). Besides, new geological evidences contradict the arguments upon which this uplift event was based: for example, the dating as Paleocene (Charrière et al., 2009) of the red-beds that overlie some of the gabbro outcrops, previously considered as Jurassic, or the clear attribution of the regional cleavage to the Cenozoic compression instead of to a Mesozoic stage (Calvín et al., 2017b). Towards the north, a Jurassic-Cretaceous continental series, topped by Cretaceous marine sediments, crop out in several basins (e.g. Bensalah et al., 2013). Moragas et al. (2016), combining new data of vitrinite reflectance, stratigraphic relationships, and subsidence curves, found that it is necessary to consider an extra burial of 1200 m corresponding to Upper Jurassic and Cretaceous sediments in the CHA.

The Cenozoic Alpine basin inversion shortened the High Atlas in a N-S direction between 15 and 24% (Teixell et al., 2003), without considering internal deformation associated with tectonic cleavage (e.g. Laville and Piqué, 1992; Calvín et al., 2017b) or the interference with Mesozoic structures (Torres-López et al. 2016). In the central sector of the CHA, the geological structure is strongly conditioned by the presence of a thick décollement level, tectonic inheritance from the Jurassic extensional stage, and the thickness variations of the Jurassic series (Fig. 2b). Therefore, tightening of Jurassic diapirs favored the accommodation of shortening; the absence of evaporites in the cores of some anticlines (being replaced by Triassic and Jurassic competent igneous rocks; Fig. 2b) can be related to extrusion and squeezing during shortening. In areas lacking salt-walls and/or

extensional structures the deformation is accommodated by minor thrusts rooted within the Jurassic sequence and folds associated with axial-plane cleavage (e.g. Calvín et al., 2017b).

3. The *ca*. 100 Ma remagnetization in the CHA

Torres-López et al. (2014) evidenced the presence of a widespread remagnetization in the CHA affecting the Jurassic carbonates. This remagnetization is characterized by its syn-tectonic behavior, systematic normal polarity with northwestern declination and positive inclination, and Albian-Cenomanian age (*ca*. 100 Ma), that has been established according to comparison with the apparent global wander path. Magnetic properties point to a chemical remagnetization, under which a population of fine magnetite grains (from superparamagnetic -SP- to stable single domain -SSD-) grew, giving a typical signature characterized by wasp-waisted hysteresis and maximum unblocking temperatures around 450-500ºC (see Elmore et al., 2012; Jackson and Swanson-Hysell, 2012; Torres-López et al., 2014). This kind of remagnetization has been related to the growth of magnetite at the expense of pyrite in presence of organic matter (Katz et al., 2000) and associated with temperature increase in the basins (e.g. Aubourg et al., 2012). In the case of the CHA, the remagnetized carbonates are located in areas with a minimum preserved thickness of 3-4 km of the syn-tectonic basin filling (Torres-López et al., 2014), which corresponds with areas where at least 2 km sediments have been eroded.

The triggering mechanism for the remagnetization is still a matter of debate: it should be related to cooling below a critical temperature at basinal scale, because no differences in magnetic properties or paleomagnetic directions can be found along the Jurassic sequence (e.g. Torres-López et al., 2014; Moussaid et al., 2015). Therefore, this quick decrease (at the geological scale) of temperature could be related either with the decay of a mantle anomaly (in case of considering a regional, plate-scale origin of remagnetization) or with partial inversion, exhumation and erosion of

the basin (when a local origin is considered). In any case, the triggering mechanism does not affect the use of the remagnetization for restoration purposes.

Similar chemical remagnetizations, both regarding magnetic behavior and age, have been recognized in other inverted intracontinental basins of the western sector of the Mediterranean Alpine System (Villalaín et al., 2003; Soto et al., 2008). A common point shared by these basins and the CHA is that they were affected by an extensional deformation during the Mesozoic (pre-remagnetization stage) and subsequently inverted by the Cenozoic, Alpine compression (post-remagnetization stage). In all of these basins, remagnetizations have been used to reconstruct the attitude of beds at the moment of the remagnetizations and to resolve geological issues, such as restoring the general geometry of the basins at the pre-compressional stage (Casas et al., 2009; Soto et al., 2011), determining the structuring age of the ridges of the CHA (Torres-López et al., 2016), restoring the geometry of pre-remagnetization folds (García-Lasanta et al., 2017) or dating the tectonic cleavage, controversial in age, in the CHA (Calvín et al., 2017b). All these issues demonstrate the applicability of remagnetizations in intracontinental basins as chronological markers to separate pre- and post-remagnetization deformation.

4. Methodology of paleomagnetic analysis

4.1. Sampling and paleomagnetic procedures

Thirty-three new sites were sampled in Jurassic carbonatic rocks using a gasoline-powered machine; twenty-one of these sites are located around the Toumliline diapir (Fig. 2). Between six and eight samples per site were thermally demagnetized by means of thermal demagnetizers TD48-DC (ASC Scientific) (TM and DP sites) and MMTD80A (Magnetic Measurements) (ILA and ILB sites) following a stepwise procedure, with 6-15 steps from room temperature up to the total

demagnetization of the specimens (usually 500-550ºC). Magnetic measurements were conducted using a 755 Superconducting Rock Magnetometer (2G). Several rock magnetic experiments (hysteresis loops, backfield curves, magnetization thermomagnetic curves, etc.) were performed using a variable field translation balance MMVFTB (Magnetic Measurements). All these experiments were carried out at the Paleomagnetic Laboratory of Burgos University (Spain).

4.2. Data processing: paleomagnetic directions, small circle analysis and structural restoration

Paleomagnetic directions were calculated using Remasoft 3.0 software (Chadima and Hrouda, 2006) by principal component analysis (Kirschvink, 1980) on orthogonal demagnetization diagrams. Mean site directions and related statistical parameters were calculated (Fisher, 1953). Rock magnetic data were analyzed with Analyzer 1.0 software (Leonhardt, 2006). Bootstrap fold-tests (Tauxe and Watson, 1994) were performed by using Pmagpy software (Tauxe et al., 2016).

Synfolding remagnetizations acquired between two deformational events can be used to reconstruct basin geometry if we assume that (i) the remagnetization was acquired at the same moment (at geological scale) within the whole basin, (ii) each bed was rotated according to a horizontal axis that coincides with its present-day strike, both during the pre- and the post-remagnetization stages and accordingly (iii) beds have not been affected either by vertical axis rotations or successive non-coaxial deformations. If these conditions are met, it is possible to calculate the remagnetization direction using the Small Circle Intersection (SCI) method (Shipunov, 1997; Henry et al., 2004; Waldhör and Appel, 2006). This method is based on the principle that the paleomagnetic direction for each site must be the same, and all possible deviations are due to tilting of the paleomagnetic directions around the bedding strike. It is then possible to find the common direction to all sites (i.e. the remagnetization direction) analyzing the small circles intersections. These small circles (SCs) are the paths followed by the paleomagnetic direction during bedding

restoration. Therefore, the small circles must intersect in a common direction that coincides with the remagnetization direction. The remagnetization direction is given with an uncertainty ellipse obtained from a population of 500 solutions beginning with a parametric bootstrap allowing propagation of errors of the in situ paleomagnetic directions and bedding (Calvín et al., 2017c).

The calculated paleomagnetic direction is used as the reference for restoring the attitude of beds at the moment of the remagnetization event, following the methodology explained in Villalaín et al. (2015). It consists in applying partial bedding corrections in order to identify the paleomagnetic direction for each site (i.e. within each small circle) in the closest orientation to the reference (i.e. the best fit direction, BFD), and in this way the paleo-dip of the bed can be easily calculated. For the case of remagnetization post-dating diapiric deformation, once the paleo-dip at *ca*. 100 Ma has been calculated, it is possible to restore the geometry of the sedimentary cover around the diapir at its pre-inversion stage. SCs methods were applied using pySCu software (Calvín et al., 2017c).

Graphical inspection of the SCs distribution gives an idea about the degree to which initial assumptions are fulfilled (Calvín et al., 2017c and references therein). However, regional tilts or vertical axis rotations that presumably involve all sites as an only block cannot be appreciated in the SC distribution. These processes can lead to erroneous interpretations of the remagnetization direction and therefore of its age (usually established by comparison with the apparent polar wander path, APWP). All in all, however, large-scale horizontal or vertical axis rotations are not crucial for the structural restoration because the selected reference for paleo-dip calculations is the same for all sites, and therefore the angular relationships between sites are preserved. In any case, fulfillment of the previous requirements in the CHA has been positively assessed in previous works (Torres-López et al., 2016; Calvín et al., 2017b).

5. Paleomagnetic results

5.1. Natural remanent magnetization (NRM) and paleomagnetic directions

NRM demagnetization diagrams (Fig. 3) show a heterogeneous behavior, characterized by intensities of 0.5-30 mA/m and several paleomagnetic components. The most common behavior (Fig. 3a) is the presence of a stable paleomagnetic component with an unblocking temperature spectrum comprised between 300 and 450ºC and intermediate coercivities (20-100 mT), hereinafter called A component (Fig. 3). This component shows systematically northwestwards declination and positive inclinations (normal polarity). In most samples, it appears together with a viscous component (Vs in figure 3) with unblocking temperatures between 100ºC and 250ºC. In some cases, in addition to components A and Vs, a low temperature (<100 ºC), high coercivity (not destroyed at 100 mT) component, called G, is also observed (fig. 3b). It is probably due to the presence of goethite. In 14 samples a high temperature component (component B; see supplementary material) that shows a direction clearly different from that of component A (fig. 3c and d) has been isolated. In some cases, as in site TM09, component B shows normal and reverse polarities coexisting with the normal component A (fig. 3c). However, in other cases such as sites LB12 and LB13, component B is patent but component A is absent (fig. 3d). The B component shows variable maximum unblocking temperatures, in most cases over 625ºC (fig 3d) and presents high coercivities (>100 mT) pointing to hematite as the mineral carrier.

A regional bootstrap fold-test (Tauxe and Watson, 1994) was performed considering components A and B (fig 4a). Component B shows an almost negative result with a range of confidence between 3% and 27% of unfolding thus pointing to a secondary origin. This is an interesting example of a secondary magnetization showing, however, normal and reverse polarities. B component was properly isolated in 14 samples and can be interpreted as syn-folding (almost

post-folding) magnetization, suggesting that it was acquired most probably after the Cenozoic compression.

On the other hand, component A shows a clear syn-folding acquisition with a maximum grouping at about 50% of unfolding (fig. 4a). This result reveals that it is a syn-folding remagnetization.

In spite of this heterogeneous behavior (even at site scale), A component was isolated in almost all sites (see supplementary material) and was therefore considered as the Characteristic Remanent Magnetization (ChRM). It shows similar features to the remagnetization observed in the surrounding areas both in terms of magnetic properties and distribution of directions (Torres-López et al., 2014; Calvín et al., 2017b): (i) Its carrier is magnetite according to rock magnetic experiments (Fig. 3e) and NRM demagnetization behavior; parameters of the hysteresis loops (Fig. 3f) correspond to a mixture of SSD and SP magnetite (Dunlop 2002), which is a typical behavior of chemical remagnetized limestones (Channel and McCabe, 1994; Jackson and Swanson-Hysell, 2012). (ii) The directions of A component show normal polarity and scattered directions before and after total bedding correction (BBC and ATBC respectively). Therefore we conclude that component A is the remagnetization described in the area by the mentioned authors and dated at *ca.* 100 Ma.

5.2 Remagnetization direction

The 32 paleomagnetic site-mean directions of the ChRM obtained in this work were analyzed together with other 68 previously published paleomagnetic directions (Torres-López et al., 2014; Calvín et al., 2017b) (Table 1) from Jurassic rocks of the neighboring area. These data have been filtered in order to use only reliable directions (directions far from the calculated reference, and therefore suspicious of not fulfilling the requirements for the SC methods, were excluded). Using the 100 paleomagnetic directions, the SCI solution was calculated with its Kent's (1982) 95%

confidence ellipse (n: 100, Dec: 332.2º, Inc: 34.5º, η: 6.2º, ξ: 2.0º, A/n: 6.427º). This direction coincides with paleomagnetic vectors obtained from two horizontal sites of the study area (AG02 and SK12, Table 1; Fig. 4), and cuts the APWP in *ca*. 100 Ma; this direction is therefore used as reference for the best fit direction (BFD) and paleo-dip calculations (Table 1). These paleo-dips have been determined for the 32 sites of this study and 16 sites of previous works (Table 1) and they are used in the next section to restore the geometry of the structures to their pre-compressional stage (*ca.* 100 Ma).

From the dispersion pattern (Fig. 4), it can be observed that all SCs have their paths close to the calculated direction, giving BFDs close to it (Table 1). This is indicative of (i) absence of differential vertical axis rotation between sites and (ii) coaxiality between pre- and post-remagnetization deformation, at least as a general rule. The angle between the reference and the BFD (Table 1) is a good indicator of the reliability for each site and of the absence of local problems that could preclude the use of some particular site for structural considerations. For example, TM07 or ILA08 have values of this angle higher than 20º.

6. Present-day and restored structure

Four ENE-WSW diapiric structures can be observed in the study area (Fig. 2), following the general structural trend. In the next subsections we present a combination of field observations, cross-sections showing the structure at present and restored at *ca.* 100 Ma through the analysis of the remagnetization (Figs. 5 to 9), and a general cross-section (with the present day and *ca*. 100 Ma attitude) merging data from individual cross-sections (Fig. 9).

6.1 The Ikkou ridge

The Ikkou structure (Figs. 2 and 5) is a tight (<1 Km wide), long salt-wall extending for several tens of kilometers along trend. In its core, Triassic basalts are dominant and in its northern outcrop there are fragments of a hook in Lower Jurassic rocks. Its present-day structure (Figs. 2 and 5a) shows that the overburden strikes sub-parallel to the salt-wall, with moderate to high dips, steeper when approaching the salt-wall. Although the presence of compressive structures is not prevalent in its S limb, its N limb shows north-verging chevron folds related to intra-Jurassic detachments (Fig. 5d). A detailed reconstruction of these folds (Fig. 5e) at *ca.* 100 Ma shows that they post-date the remagnetization, and are therefore related to the Cenozoic compression. In the restoration of the Ikkou ridge (Fig. 5b) it can be observed that most of the tilting of the limbs was already developed during the extensional stage (with the exception of chevrons folds), with moderate dips of beds close to the ridge and showing a rapid decrease of dip with increasing distance from the ridge (compare DP10 and 11 with ILA sites, Fig. 5b). According to previous works (Torres-López et al., 2016; Calvín et al., 2017b) in the Ikkou syncline it was already developed during the extensional stage and was tightened during the Cenozoic, developing a N-verging thrust and subvertical cleavage. We interpret that, as it occurs in the cross-sections across the Ikkou syncline (Calvín et al., 2017b), the squeezing of the salt-wall was associated with north-verging thrusting (Fig. 5a). This is in agreement with the rotation path recorded by gabbros (Calvín et al., 2017a) that crop out in the core of some of these ridges (i.e. Tasraft, Tassent, Tirrhist and Anefgou ridges). Although it is not possible to estimate the original width of the salt-wall during the pre-compressional stage, the almost absence of shales and salt in its core indicates that it was wider and was totally welded during the Cenozoic compression.

Differences in thickness can be observed between the Bajocian levels at both limbs of the ridge, being thicker in its N limb. However, the opposite happens regarding the Bathonian-Callovian redbeds, which are thicker in the S limb. An unconformity at the base of the redbeds is

especially evident close to the southern limb of the Ikkou ridge, indicating a change in the diapiric/subsidence activity.

6.2 The Tadaghmamt ridge

The Tadaghmamt salt-wall (Figs. 2 and 6) is elongated in an ENE-WSW direction and about 10 km long and 1-2 km wide. Its core consists of both sedimentary and volcanic Triassic rocks. The Jurassic series shows low to moderate dips, and is strongly folded towards the NE, where the Tissila anticline is located (Fig. 2). The overall structure can be followed more than 100 km along trend, relaying with other folds towards the SW. For example, the Tadaghmamt ridge connects with the Azourki Ridge (Vergés et al. 2017), through a N-dipping normal fault system and small diapirs. Towards the NE, the Tadaghmamt anticline ends without evidence of continuity or relay with other structures.

The N limb of the Tadaghmamt ridge is generally subhorizontal, although it shows decametric-scale south-verging folds and increasing dips close to the ridge axis. In the core of the ridge, Triassic basalts (mainly in the NE sector) and shales (along all the salt-wall), both capped by Bajocian limestones (Fig. 6d, e), crop out. The latter have been differentially folded, showing both gentle and tight folds. The S limb is characterized by the presence of a kilometer-scale, north-verging asymmetric anticline; its N limb presents moderate dips (Fig. 6f) whereas its S limb shows low-to moderate dips that become sub-horizontal a few kilometers from the ridge (Fig. 6a). It is curious that both DP13 and ILB06 (dipping away from the ridge axis during the basinal stage), changed their sense of dip during compression (Fig. 6b) and show moderate dips towards the ridge rapidly changing near the thrust (DP13) or defining a secondary anticline (ILB06).

6.3 The Timedouine ridge

The Timedouine salt-wall (Figs. 2 and 7) is the NE end of a 50 Km NE-SW to NNE-SSW striking, S-dipping normal fault system. The Ikerzi and Moussa diapirs (Fig. 1) and the Msemrir Bathonian-Callovian basin (Ettaki et al., 2007) are also associated with this fault system. The Timedouine structure is 13 km long, 1 km wide, and shows a NE-SW trend; it is cored by Triassic shales and basalts, and scarce outcrops of Jurassic gabbros. The presence of gabbros probably evidences its connection with a basement fault. The Mesozoic sedimentary cover is gently folded close to the ridge with low to moderate dips and folds in both limbs verging towards the ridge (Fig. 7a), and becoming subhorizontal at around 1 km from the salt-wall. In the eastern end of the ridge, compressional structures are more pervasive, and hectometer-scale monoclines verging towards the ridge (Fig. 2b) and recumbent folds associated with detachments from the core of the ridge appear. In this area, slumps and local sedimentary unconformities in the Aalenian-Bajocian marls can be observed (Fig. 7e).

When the geometry of the overburden is restored (Fig. 7b) the structure is similar to the one observed in the Tadaghmamt ridge, with steep to moderate dips close to the ridge that rapidly become subhorizontal away from it.

6.4 The Toumliline ridge

Finally, Toumliline (Figs. 2 and 8) is a 5 x 1 km diapiric structure, elongated along the main structural trend, and related to a north-dipping basement normal fault (Fig. 2) (Teixell et al., 2003). Large amounts of salt, which has been the object of traditional exploitation (the name ‘Toumliline’ refers in the tamazight autochthonous language to the white color of the salt), crop out in its core. Besides, Triassic basalt and Jurassic gabbros can be recognized in the center of the diapir,

suggesting a synformal structure. The Jurassic cover shows moderate to steep dips when approaching the core in the northern limb of the diapiric structure and shallow to moderate dips in its southern limb (Fig. 8a). Towards the WSW and ENE, the diapir ends and a north verging thrust can be observed superposing the Lower Jurassic over the Middle Jurassic rocks (Fig. 8d). The *ca.* 100 Ma structure shows a similar attitude but shallower dips. In the hanging wall, the paleo-dips obtained in the marls (Fig. 8b) change very quickly and this can be probably related to growth strata in this unit, although a section perpendicular to the fault would be needed to confirm this issue. In the footwall, the paleomagnetic sites close to the core show low dips towards the S (Fig. 8b, sites TM05, 07, 08, 09) whereas the farthest paleomagnetic site (IC54) presents a shallow northwards dip, defining a gentle syncline. This is consistent with salt migration during the extensional stage and the development of a salt-roller. The cross-section made towards the NE (Fig. 8e) cuts across a non-diapiric zone, and shows the lower part of the thrust that can be observed towards the SW; in the restored cross-section this thrust shows shallow dips. The restored structure shows that the folds associated with the north-verging thrust were developed during the Cenozoic, because they do not appear in the *ca.* 100 Ma structure, which in turn is similar to the section that cuts across the diapir (Fig. 8a).

7. Interpretation

Recent research works (Saura et al., 2014; Moragas et al., 2016; Martín-Martín et al., 2017, Teixell et al. 2017; Vergés at al., 2017) evidence the major role of salt tectonics in the development of sedimentary basins during the Early-Middle Jurassic in the CHA. Jurassic subsidence was conditioned mainly by extensional tectonics, but with a significant contribution of salt migration (Moragas et al., 2016). During the Cenozoic compression these salt-walls accommodated the shortening and some of them were strongly tightened (e.g. Teixell et al., 2017), erasing the evidence

of salt-tectonics and extension-related processes. Exceptions are the salt-walls that contain more competent rocks (Jurassic hooks, Triassic basalts and Jurassic gabbros) or structures having a post-compressional halokinetic activity. Following this line, the ridge linked to the Toumliline diapir (its prolongation towards the NE) could be a priori interpreted as a welded Jurassic salt-wall, since its present shape shows upright limbs limited by a tectonic contact (Fig. 8e). Although its present-day geometry is similar to the Ikkou ridge (in this case without Triassic basalt between both limbs), the *ca.* 100 Ma restoration indicates that most of the tilting associated with the Toumliline ridge is Cenozoic in age. This is an example of how paleomagnetic results and quantification of the paleo-dips can help to achieve a more accurate interpretation about the evolution of this kind of structures.

The comparison between the pre- and post- compressional structure (*ca.* 100 Ma restored and present day, respectively) sheds light into the meaning of diapiric processes as generators of the CHA ridges and into the mechanisms by which the inherited extensional structures conditioned their compressional geometry. The analyzed structures show differences regarding the two stages of development related to their evolution (Fig. 9).

7.1 Implications for ridges development

Although in a simplistic view the ridges found in the CHA can be interpreted as welded salt-walls limiting minibasins, a detailed analysis of the four structures that crop out between the localities of Imilchil and Toumliline indicates strong differences regarding both their present-day geometry and their pre-compressional structure. This indicates contrasting evolutions during the extensional and compressional stages.

The Ikkou ridge shows similar geometry of the Jurassic sedimentary cover before and after the Cenozoic compression, with steeply-dipping Jurassic beds at both stages. The Cenozoic deformation in this ridge is restricted to tightening of the salt-wall (as much as allowed by the

presence of competent rocks, such as basalts or gabbros in its core) together with north-verging thrusting, development of cleavage in both limbs (especially in the southern one) and minor, north-verging folds in the footwall of the thrust (Figs. 5 and 9). The Mesozoic deformation (Fig. 9b) consisted in the uplift of the core and outwards, centrifuges tilting in the first 1-2 km away from it at the limbs, with a quick decrease of the paleo-dip towards the synclines. This scenario agrees with the presence of a salt-wall limiting sedimentary depocenters during the Jurassic. The Mesozoic salt-wall cuts the sedimentary pile up to the Bathonian-Callovian redbeds, whose shallow dips in the NW limb of the Ikkou syncline and their basal unconformity point to a decreasing rate of salt migration in the salt-wall during the sedimentation of the redbeds. This can suggest that this unit could have fossilized the salt-wall. On the other hand, the Tadaghmamt and Timedouine salt-walls share similar features that differ from the Ikkou and Toumliline structures. In this central sector, the structure is characterized by flat-lying beds of Bajocian limestones that top the Triassic basalts and shales in the core of the Tadaghmamt ridge. Close to the ridge axes, the limbs are complicated by minor, decameter- to hectometer-scale folds as a consequence of buttresing towards the ridge during the Cenozoic compression. Conversely, their Mesozoic attitude was characterized by tilting of the limbs away from the ridge affecting only the area adjacent to the salt-walls (Fig. 9). This small tilting and the fact that the salt-walls do not completely cut through the Bajocian limestones seem to indicate lower extensional activity and consequently lower salt migration in the Tadaghmamt and Timedouine ridges.

The Jurassic cover of the Toumliline ridge shows shallow dips in the restored section, with exception of sites located in the hanging wall of the normal fault (Figs. 8 and 9). Furthermore, shortening of the Toumliline diapir during the Cenozoic was important, generating thrust-related folds. The cross-section of the ridge towards the W of the diapir depicts similar features, showing shallow dips in the pre-compressional restoration. Therefore, this structure can be interpreted as a Mesozoic salt-roller related to the normal fault, without imposing major controls on the sedimentary

conditions with exception of the accommodation space generated by migration of salt from the hanging wall to the footwall. During the Cenozoic, both the presence of the normal fault and salt accumulation along the structure would favor the nucleation of deformation, generating folds and thrusts and the partial extrusion of salts forming the Toumliline diapir. Otherwise, the weaker development of Jurassic halokinetic processes in this structure can be responsible for the presence, at present, of a large amount of salt below the diapir, almost absent in other structures (e.g. the Ikkou salt-wall).

According to the comparison between the pre- and post-compressional structure, it is remarkable how the overburden and the salt-bodies themselves responded differently to the Cenozoic compression, a behavior that depends in its turn on the geometries inherited from the extensional stage, that we can summarize in three categories: (i) The Ikkou salt-wall is a well-developed Mesozoic structure whose limbs tend to show moderate to steep dips; during shortening, accommodation of the deformation occurred mainly by squeezing of the salt core accompanied by north-directed thrusting and secondary steepening of its limbs (Fig. 9). (ii) When Mesozoic deformation was gentler (as in the case of the Tadaghmamt and Timedouine structures) and only consisted in the development of a salt-wall with minor vertical movements between limbs, the development of major compressional structures during the Cenozoic stage could be difficult due to the thickness of the sedimentary series. In this case, deformation was limited to the squeezing of salt-walls and development of folds close to the ridge by buttresing (Fig. 9). (iii) Finally, the Toumliline diapir shows a different compressional style in which the development of a main thrust was favored by the pre-compressional geometry, consisting of (a) a normal fault imposing a strong throw between the future fold limbs (note that this is the only sector where the Hettangian beds crop out) and (b) a significant accumulation of salts below the hanging wall of the Cenozoic thrust. Both conditioners are related to the existence of a Mesozoic salt-roller.

7.2. Subsidence implications

Another interesting issue concerns the differences in thickness of the sedimentary pile observed between the limbs of the Ikkou and the Toumliline ridges, both related to north-dipping basement normal faults (Fig. 9). This favored higher subsidence and accumulation of sediments in the hanging wall during the Early-Middle Jurassic, evident in the Toarcian-Aalenian beds of the Toumliline ridge and the Aalenian-Bajocian beds of the Ikkou structure (Figs. 5, 8 and 9). Tectonic subsidence during this early stage, according to Moragas et al. (2016), would be complemented by salt migration from the hanging wall to the footwall.

This scenario changed during the Bathonian-Callovian redbeds deposition, contemporary with decreasing extensional activity and salt migration from the hanging wall. At this moment, the beginning of migration of the salt in the footwall favored a stronger subsidence in the S limb of the Ikkou ridge, with the generation of syncline which acted as depocenter for the redbeds (Fig. 9b). The unconformity below the redbeds could be conditioned by this change in the subsidence behavior. Furthermore, the first stage of subsidence, controlled by basement normal faults, is more continuous along strike, whereas the second stage is restricted to small areas (e.g. the Ikkou syncline), because they depended on the amount of salt (or salt migration) below the ridge, which could be heterogeneously distributed. This is evident in the western end of the Ikkou syncline; towards the W, the Jurassic shows a subhorizontal attitude, indicating the pinchout of the depocenter. Although there are not outcrops of red-beds in the Toumliline diapir to confirm this issue, following the observations of the Ikkou ridge, the syncline located in the footwall of the Toumliline ridge could have been structured during the same time.

7.3. General structure

The minimum width that ridges must have had before the compressional stage is related to the dip of the limbs in each structure: the higher the extensional tilting and the distance of affection to the limbs, the greater must be the minimum original width of the ridges. This allows to estimate the minimum shortening recorded by each individual structure during the Cenozoic compression (Fig. 9).

Tadaghmamt and Timedouine salt-walls show the lowest shortening values, around 15 % that agree with the shallow dips observed around these structures. This is also consistent with the interpretation of ridge squeezing and the development of folds in the areas adjacent to the core. The Toumliline structure shows about 20 % of minimum shortening but this figure strongly depends on the amount of displacement accommodated by the thrust, which is poorly constrained and could be higher than interpreted in this cross-section. Finally, the minimum width is greater for the Ikkou salt-wall than for the other structures and therefore it shows the highest shortening value, which is mainly accommodated by the squeezing of the salt-wall. In an overall view, the mean estimated shortening is around 19 %, what agrees with average shortening values proposed for the entire chain along this cross-section (Teixell et al., 2003).

An interesting issue is the accommodation of deformation at deeper levels, within the Paleozoic basement. Although geometry of structures at this level is conjectural, its present-day envelope agrees with the one adjusted by means of a gravimetric section (Ayarza et al. 2005). This envelope is characterized in the study area by two well differentiated structural highs, whose limit is the monocline south of the Ikkou syncline. Considering only the present-day dips, it is reasonable to interpret this geometry as a consequence of a north-verging basement thrust, with an associated hanging wall fold represented by the observed monocline. In fact, these variations in structural depth of the top of the basement have been previously interpreted as an evidence of the involvement of the basement in the compressional structure (Teixell et al., 2003). However, the restored cross-

section shows that these variations are inherited from the basinal stage. This implies that vertical movements of the basement were important during the extension, whereas during the inversion the shortening would be probably limited to folding and steepening of previous normal faults and/or cleavage development.

8. Conclusions

The carbonate rocks that crop out between the Imilchil and Toumliline villages (Central High Atlas) show a chemical remagnetization, carried by magnetite. This paleomagnetic signal shows features similar to those observed in close areas of the CHA (Torres-López et al., 2014; Calvín et al., 2017b): maximum unblocking temperatures around 450-500ºC, site-mean paleomagnetic directions with systematically northwestwards, positive inclinations, and scattering both before and after total bedding correction. This remagnetization was dated as *ca.* 100 Ma (Torres-López et al., 2014) from comparison with the apparent polar wander path of North Africa (Torsvik et al., 2012).

By means of the small circle method, the geometry of the overburden of four salt-related structures has been quantitatively restored to the moment of the acquisition of the remagnetization (*ca.* 100 Ma, i.e. a tectonic quiescence period predating the Cenozoic compression). This methodology appears to be promisingly useful in the study of diapiric salt structures because allows to analyze the structure derived directly from the halokinetic processes generated during the basinal stage, without the subsequent compressional imprint.

Specifically, the application of paleomagnetic methodology in four structures of the CHA returns the following conclusions:

- Most of the paleomagnetic directions, once they are restored at the remagnetization time, are close to the reference direction. This is indicative of the absence of significant and generalized vertical

axis rotations and/or non-coaxial deformation during the pre- and post-remagnetization deformation stages.

- The Ikkou salt-wall was almost totally developed during the extensional stage; the *ca.* 100 Ma restored geometry shows moderate to steep dips of the cover rocks, subparallel to the salt-wall, and similar attitude to the present-day structure. Cenozoic compression resulted in the squeezing and extrusion of its saline core (only Triassic basalts remain at present) together with north-directed thrusting, cleavage development and folding.

- In the Timedouine and Tadaghmamt ridges only Bajocian limestones crop out; in the case of the Timedouine ridge, they do not allow to reconstruct the pre-compressional evolution of the salt-walls. However, the extensional geometries of both ridges show moderate dips away from their cores, indicating that the salt-walls were already developed before the remagnetization acquisition. In these ridges, the Jurassic deformation was minor, confined to the areas adjacent to the structure; the Cenozoic compression only generated the welding of the salt-walls and buttressing of the overburden towards the structures, with the generation of folds verging towards the ridges.

- The *ca.* 100 Ma structure of the Toumliline diapir was mainly conditioned by normal faulting; the hanging wall is deformed close to the fault, showing growth strata or a drag fold, whereas the rocks of the footwall are deformed by a salt-roller. Most of the present-day structure developed during the Cenozoic compression, whit the development of a north-verging thrust and associated folds.

Acknowledgements

Special thanks to B. Oliva, E. Sánchez, Á. Herrejón and T. Mochales for their kind help during field work. The authors are grateful for their comments and suggestion to two anonymous reviewers as well as to the editor Rob Govers.

Funding

This study was supported by the MINECO (Spanish Ministry of Economy and Competitiveness) cofinanced by the ERDF (European Union) (research projects CGL2012-38481 and CGL2016-77560). PC also acknowledges the MINECO (F.P.I. research grant BES-2013-062988).

References

Armando, G., 1999. Intracontinental alkaline magmatism: Geology, Petrography, Mineralogy and Geochemistry of the Jebel Hayim Massif (Central High Atlas-Morocco). Mémories de Géologie de l'Université de Lausanne 31, 106.

Aubourg, C., Pozzi, J., Kars, M., 2012. Burial, claystones remagnetization and some consequences for magnetostratigraphy. Geol. Soc. London, Spec. Publ. 371, 181–188. doi:10.1144/SP371.4

Ayarza, P., Alvarez-Lobato, F., Teixell, a., Arboleya, M.L., Tesón, E., Julivert, M., Charroud, M., 2005. Crustal structure under the central High Atlas Mountains (Morocco) from geological and gravity data. Tectonophysics 400, 67–84. doi:10.1016/j.tecto.2005.02.009

Barbero, L., Teixell, A., Arboleya, M.-L., Río, P. Del, Reiners, P.W., Bougadir, B., 2007. Jurassic-to-present thermal history of the central High Atlas (Morocco) assessed by low-temperature thermochronology. Terra Nov. 19, 58–64. doi:10.1111/j.1365-3121.2006.00715.x

Beauchamp, W., Allmendinger, R.W., Barazangi, M., Demnati, A., El-Alji, M., Dahmani, M., 1999. Inversion tectonics and the evolution of hte High Atlas Mountains, Morocco, based on a geological-geophysical transect. Tectonics 18, 163–184.

Borradaile, G.J., 1997. Deformation and paleomagnetism. Surv. Geophys. 18, 405–436. doi:10.1023/A:1006555906559

Bouchouata, A., Canérot, J., Souhel, A., Gharib, A., 1995. Stratigraphie séquentielle et évolution géodynamique du Jurassique de la région Talmest-Tazoult (Haut Atlas central, Maroc). Comptes Rendus L'Academie Des Sci. Paris 320, 749–756.

Calvín, P., Casas-Sainz, A.M., Villalaín, J.J., Moussaid, B., 2017. Diachronous folding and cleavage in an intraplate setting (Central High Atlas, Morocco) determined through the study of remagnetizations. J. Struct. Geol. 97, 144–160. doi:10.1016/j.jsg.2017.02.009

Calvín, P., Ruiz-Martínez, V.C., Villalaín, J.J., Casas-Sainz, A.M., Moussaid, B., 2017. Emplacement and Deformation of Mesozoic Gabbros of the High Atlas (Morocco): Paleomagnetism and Magnetic Fabrics. Tectonics. doi:10.1002/2017TC004578

Calvín, P., Villalaín, J.J., Casas-Sainz, A.M., Tauxe, L., Torres-López, S., 2017. pySCu: a new python code for analyzing remagnetizations directions by means of Small Circle utilities. Comput. Geosci. 109. doi:10.1016/j.cageo.2017.07.002

Casas, A.M., Villalaín, J.J., Soto, R., Gil-Imaz, A., del Río, P., Fernández, G., 2009. Multidisciplinary approach to an extensional syncline model for the Mesozoic Cameros Basin (N Spain). Tectonophysics 470, 3–20. doi:10.1016/j.tecto.2008.04.020

Chadima, M., Hrouda, F., 2006. Remasoft 3.0 a user-friendly paleomagnetic data browser and analyzer. Trav. Géophysiques 27, 20–21.

Channell, J.E.T., McCabe, C., 1994. Comparison of magnetic hysteresis parameters of unremagnetized and remagnetized limestones. J. Geophys. Res. Solid Earth 99, 4613–4623. doi:10.1029/93JB02578

Charrière, A., 1990. Héritage hercynien et évolution géodynamique alpine d'une chaîne intracontinentale: le Moyen Atlas au SE de Fès (Maroc). Univ. Paul-Sabatier Toulouse.

Costa, E., Vendeville, B.C., 2002. Experimental insights on the geometry and kinematics of fold-and-thrust belts above weak, viscous evaporitic décollement. J. Struct. Geol. 24, 1729–1739. doi:10.1016/S0191-8141(01)00169-9

Davis, D.M., Engelder, T., 1985. The role of salt in fold-and-thrust belts. Tectonophysics 119, 67–88. doi:10.1016/0040-1951(85)90033-2

Domènech, M., Teixell, A., Babault, J., Arboleya, M.-L., 2015. The inverted Triassic rift of the Marrakech High Atlas: A reappraisal of basin geometries and faulting histories. Tectonophysics. doi:10.1016/j.tecto.2015.03.017

Dunlop, D.J., 2002. Theory and application of the Day plot (M rs / M s versus H cr / H c) 2. Application to data for rocks, sediments, and soils. J. Geophys. Res. 107, 2057. doi:10.1029/2001JB000487

Elmore, R.D., Muxworthy, a. R., Aldana, M., 2012. Remagnetization and chemical alteration of sedimentary rocks. Geol. Soc. London, Spec. Publ. 371, 1–21. doi:10.1144/SP371.15

Ettaki, M., Ibouh, H., Chellaï, E.H., Milhi, 2007. Les structures "diapiriques" liasiques du Haut-Atlas central, Maroc: example de la ride d`Ikerzi. Africa Geosci. Rev. 14, 79–93.

Fadile, A., 2003. Carte géologique du Maroc à 1/100 000, feuille Imilchil. Notes Mém. Serv. géol. Maroc 397.

Ferrer, O., Jackson, M.P.A., Roca, E., Rubinat, M., 2012. Evolution of salt structures during extension and inversion of the Offshore Parentis Basin (Eastern Bay of Biscay). Geol. Soc. London, Spec. Publ. 363, 361–379. doi:10.1144/SP363.16

Fisher, R., 1953. Dispersion on a Sphere. Proc. R. Soc. A Math. Phys. Eng. Sci. 217, 295–305. doi:10.1098/rspa.1953.0064

Fletcher, R.C., 1974. Wavelength selection in the folding of a single layer with power-law rheology. Am. J. Sci. 274, 1029–1043. doi:10.2475/ajs.274.9.1029

Frizon de Lamotte, D., Zizi, M., Missenard, Y., Hadif, M., El Azzouzi, M., Maury, R.C., Charrière, A., Taki, Z., Benammi, M., Michard, A., Hafid, M., Azzouzi, M. El, Maury, R.C., Charrière, A., Taki, Z., Benammi, M., Michard, A., 2008. The Atlas System, in: Michard, A., Saddiqi, O., Chalouan, A., Lamotte, D. de F. (Eds.), Continental Evolution: The Geology of Morocco. Lecture Notes in Earth Sciences 116. Springer, Berlin, Heidelberg, pp. 133–202. doi:10.1007/978-3-540-77076-3_4

García-Lasanta, C., Casas-Sainz, A., Villalaín, J.J., Oliva-Urcia, B., Mochales, T., Speranza, F., 2017. Remagnetizations used to unravel large-scale fold kinematics: a case study in the Cameros basin (N Spain). Tectonics. doi:10.1002/2016TC004459

Giles, K.A., Lawton, T.F., 2002. Halokinetic sequence stratigraphy adjacent to the El Papalote diapir, Northeastern Mexico. Am. Assoc. Pet. Geol. Bull. 86, 823–840. doi:10.1306/61EEDBAC-173E-11D7-8645000102C1865D

Gomez, F., Beauchamp, W., Barazangi, M., 2000. Role of the Atlas Mountains (northwest Africa) within the African-Eurasian plate-boundary zone. Geology 28, 775. doi:10.1130/0091-7613(2000)28<775:ROTAMN>2.0.CO;2

Hadri, M., 1997. Carte géologique du Maroc à 1/100 000, feuille Tinejdad. Notes Mém. Serv. géol. Maroc1 385.

Hailwood, E. a., Mitchell, J.G., 1971. Palaeomagnetic and Radiometric Dating Results from Jurassic Intrusions in South Morocco. Geophys. J. Int. 24, 351–364. doi:10.1111/j.1365-246X.1971.tb02183.x

Heitzmann, P., Stüder, M.A., 1990. Carte géologique du Maroc au 1/100000, feuille Tounfite. Notes Mém. Serv. géol. Maroc 357.

Henry, B., Rouvier, H., Le Goff, M., 2004. Using syntectonic remagnetizations for fold geometry and vertical axis rotation: the example of the Cévennes border (France). Geophys. J. Int. 157, 1061–1070. doi:10.1111/j.1365-246X.2004.02277.x

Henry, B., Rouvier, H., Le Goff, M., Smati, A., Hatira, N., Laatar, E., Mansouri, A., Perthuisot, V., 2000. Paleomagnetism as a structural polarity criterion: Application to Tunisian diapirs. J. Struct. Geol. 22, 323–334. doi:10.1016/S0191-8141(99)00155-8

Jackson, C.A.L., Lewis, M.M., 2016. Structural style and evolution of a salt-influenced rift basin margin; the impact of variations in salt composition and the role of polyphase extension. Basin Res. 28, 81–102. doi:10.1111/bre.12099

Jackson, M., Swanson-Hysell, N.L., 2012. Rock magnetism of remagnetized carbonate rocks: another look. Geol. Soc. London, Spec. Publ. 371, 229–251. doi:10.1144/sp371.3

Joussiane, R., 2016. Les relations entre diapirisme et sédimentation: Exemple du Jurassique moyen de la région d'Imilchil, Haut-Atlas central, Maroc. Université Bordeaux Montaigne.

Katz, B., Elmore, R.D., Cogoini, M., Engel, M.H., Ferry, S., 2000. Associations between burial diagenesis of smectite, chemical remagnetization, and magnetite authigenesis in the Vocontian trough, SE France. J. Geophys. Res. Solid Earth 105, 851–868. doi:10.1029/1999JB900309

Kent, J.T., 1982. The Fisher-Bingham distribution on the sphere. J. R. Stat. Soc. Ser. B 44, 71–80.

Kirschvink, J.L., 1980. The least-squares line and plane and the analysis of paleomagnetic data. Geophys. J. R. Astron. Soc. 62, 699–718. doi:10.1111/j.1365-246X.1980.tb02601.x

Knight, K.B., Nomade, S., Renne, P.R., Marzoli, A., Bertrand, H., Youbi, N., 2004. The Central Atlantic Magmatic Province at the Triassic-Jurassic boundary: paleomagnetic and 40Ar/39 Ar evidence from Morocco for brief, episodic volcanism. Earth Planet. Sci. Lett. 228, 1–2.

Kocher, T., Schmalholz, S.M., Mancktelow, N.S., 2006. Impact of mechanical anisotropy and power-law rheology on single layer folding. Tectonophysics 421, 71–87. doi:10.1016/j.tecto.2006.04.014

Laville, E., Piqué, A., 1992. Jurassic penetrative deformation and Cenozoic uplift in the Central High Atlas (Morocco): A tectonic model. structural and orogenic inversions. Geol. Rundschau 81, 157–170. doi:10.1007/BF01764546

Leonhardt, R., 2006. Analyzing rock magnetic measurements: The RockMagAnalyzer 1.0 software. Comput. Geosci. 32, 1420–1431.

Malaval, M., 2016. Enregistrement sédimentaire de l'activité diapirique associée à la ride du Jbel Azourki. Haut-Atlas Central, Maroc. Enregistrement sédimentaire de l'activité diapirique associée à la ride du Jbel Azourki. Haut-Atlas Central, Maroc.

Martín-Martín, J.D., Vergés, J., Saura, E., Moragas, M., Messager, G., Baqués, V., Razin, P., Grélaud, C., Malaval, M., Joussiaume, R., Casciello, E., Cruz-Orosa, I., Hunt, D.W., 2017. Diapiric growth within an Early Jurassic rift basin: The Tazoult salt wall (central High Atlas, Morocco). Tectonics 36, 2–32. doi:10.1002/2016TC004300

Mattauer, M., Tapponnier, P., Proust, F., 1977. Sur les mecanismes de formation des chaines intracontinentales; l'exemple des chaines atlasiques du Maroc. Bull. la Soc. Geol. Fr. S7–XIX, 521–526. doi:10.2113/gssgfbull.S7-XIX.3.521

Michard, A., 1976. Eléments de gélogie marocaine. Notes Mém. Serv. Géol. Maroc 252, 408 pp.

Michard, A., Ibouh, H., Charrière, A., 2011. Syncline-topped anticlinal ridges from the High Atlas: A Moroccan conundrum, and inspiring structures from the Syrian Arc, Israel. Terra Nov. 23, 314–323. doi:10.1111/j.1365-3121.2011.01016.x

Milhi, A., 1997. Carte géologique du Maroc à 1/100 000, feuille Tinghir. Notes Mém. Serv. géol. Maroc 377.

Moragas, M., Vergés, J., Nalpas, T., Saura, E., Martín-Martín, J.D., Messager, G., Hunt, D.W., 2017. The impact of syn- and post-extension prograding sedimentation on the development of salt-related rift basins and their inversion: Clues from analogue modelling. Mar. Pet. Geol. 88, 985–1003. doi:10.1016/j.marpetgeo.2017.10.001

Moragas, M., Vergés, J., Saura, E., Martín-Martín, J.-D., Messager, G., Merino-Tomé, Ó., Suárez-Ruiz, I., Razin, P., Grélaud, C., Malaval, M., Joussiaume, R., Hunt, D.W., 2016. Jurassic rifting to post-rift subsidence analysis in the Central High Atlas and its relation to salt diapirism. Basin Res. 1–27. doi:10.1111/bre.12223

Moussaid, B., Villalaín, J.J., Casas-Sainz, A., El Ouardi, H., Oliva-Urcia, B., Soto, R., Román-Berdiel, T., Torres-López, S., 2015. Primary vs. secondary curved fold axes: Deciphering the origin of the Aït Attab syncline (Moroccan High Atlas) using paleomagnetic data. J. Struct. Geol. 70, 65–77. doi:10.1016/j.jsg.2014.11.004

Roca, E., Beamud, E., Rubinat, M., Soto, R., Ferrer, O., 2013. Paleomagnetic and inner diapiric structural constraints on the kinematic evolution of a salt-wall: The Bicorb-Quesa and northern Navarrés salt-wall segments case (Prebetic Zone, SE Iberia). J. Struct. Geol. 52, 80–95. doi:10.1016/j.jsg.2013.04.003

Santolaria, P., Vendeville, B.C., Graveleau, F., Soto, R., Casas-Sainz, A., 2015. Double evaporitic décollements: Influence of pinch-out overlapping in experimental thrust wedges. J. Struct. Geol. 76, 35–51. doi:10.1016/j.jsg.2015.04.002

Saura, E., Vergés, J., Martín-Martín, J.D., Messager, G., Moragas, M., Razin, P., Grélaud, C., Joussiaume, R., Malaval, M., Homke, S., Hunt, D.W., 2014. Syn- to post-rift diapirism and minibasins of the Central High Atlas (Morocco): the changing face of a mountain belt. J. Geol. Soc. London. 171, 97–105. doi:10.1144/jgs2013-079

Schaer, J.P., 1987. Evolution and structure of the High Atlas of Morocco, in: Schaer, J.P., Rodgers, J. (Eds.), The Anatomy of Mountain Ranges. Princeton University Press, pp. 107–128.

Shipunov, S. V, 1997. Synfolding magnetization: detection, testing and geological applications. Geophys. J. Int. 130, 405–410. doi:10.1111/j.1365-246X.1997.tb05656.x

Soto, R., Casas-Sainz, A.M., Villalain, J.J., 2011. Widespread Cretaceous inversion event in northern Spain: evidence from subsurface and palaeomagnetic data. J. Geol. Soc. London. 168, 899–912. doi:10.1144/0016-76492010-072

Soto, R., Beamud, E., Roca, E., Carola, E., Almar, Y., 2017. Distinguishing the effect of diapir growth on magnetic fabrics of syn-diapiric overburden rocks: Basque-Cantabrian basin, Northern Spain. Terra Nov. 38, 42–49. doi:10.1111/ter.12262

Soto, R., Villalaín, J.J., Casas-Sainz, A.M., 2008. Remagnetizations as a tool to analyze the tectonic history of inverted sedimentary basins: A case study from the Basque-Cantabrian basin (north Spain). Tectonics 27, n/a-n/a. doi:10.1029/2007TC002208

Tauxe, L., Shaar, R., Jonestrask, L., Swanson-Hysell, N.L., Minnett, R., Koppers, A.A.P., Constable, C.G., Jarboe, N., Gaastra, K., Fairchild, L., 2016. PmagPy: Software package for

paleomagnetic data analysis and a bridge to the Magnetics Information Consortium (MagIC) Database. Geochemistry, Geophys. Geosystems 17, 2450–2463. doi:10.1002/2016GC006307

Tauxe, L., Watson, G.S., 1994. The fold test: an eigen analysis approach. Earth Planet. Sci. Lett. 122, 331–341. doi:10.1016/0012-821X(94)90006-X

Teixell, A., Arboleya, M.-L., Julivert, M., Charroud, M., 2003. Tectonic shortening and topography in the central High Atlas (Morocco). Tectonics 22, 1051. doi:10.1029/2002TC001460

Teixell, A., Barnolas, A., Rosales, I., Arboleya, M.-L., 2017. Structural and facies architecture of a diapir-related carbonate minibasin (lower and middle Jurassic, High Atlas, Morocco). Mar. Pet. Geol. 81, 334–360. doi:10.1016/j.marpetgeo.2017.01.003

Torres-López, S., Villalaín, J.J., Casas, A.M., EL Ouardi, H., Moussaid, B., Ruiz-Martínez, V.C., 2014. Widespread Cretaceous secondary magnetization in the High Atlas (Morocco). A common origin for the Cretaceous remagnetizations in the western Tethys? J. Geol. Soc. London. 171, 673–687. doi:10.1144/jgs2013-107

Torres-López, S., Casas, A.M., Villalaín, J.J., El Ouardi, H., Moussaid, B., 2016. Pre-Cenomanian vs. Cenozoic folding in the High Atlas revealed by palaeomagnetic data. Terra Nov. 28, 110–119. doi:10.1111/ter.12197

Torsvik, T.H., Van der Voo, R., Preeden, U., Niocaill, C. Mac, Steinberger, B., Doubrovine, P. V., van Hinsbergen, D.J.J., Domeier, M., Gaina, C., Tohver, E., Meert, J.G., McCausland, P.J. a, Cocks, L.R.M., 2012. Phanerozoic polar wander, palaeogeography and dynamics. Earth-Science Rev. 114, 325–368. doi:10.1016/j.earscirev.2012.06.002

Vendeville, B.C., Jackson, M.P.A., 1992. The rise of diapirs during thin-skinned extension\rSpecial issue; salt tectonics. Mar. Pet. Geol. 9, 331–353. doi:10.1016/0264-8172(92)90047-I

Vergés, J., Moragas, M., Martín-Martín, J.D., Saura, E., Casciello, E., Razin, P., Grelaud, C., Malaval, M., Joussiame, R., Messager, G., Sharp, I., Hunt, D.W., 2017. Salt Tectonics in the Atlas Mountains of Morocco. Permo-Triassic Salt Prov. Eur. North Africa Atl. Margins 563–579. doi:10.1016/B978-0-12-809417-4.00027-6

Villalaín, J., Fernández-González, G., Casas, A.M., Gil-Imaz, A., 2003. Evidence of a Cretaceous remagnetization in the Cameros Basin (North Spain): implications for basin geometry. Tectonophysics 377, 101–117. doi:10.1016/j.tecto.2003.08.024

Villalaín, J.J., Casas-Sainz, A.M., Soto, R., 2016. Reconstruction of inverted sedimentary basins from syn-tectonic remagnetizations. A methodological proposal. Geol. Soc. London, Spec. Publ. 425, 233–246. doi:10.1144/SP425.10

Waldhör, M., Appel, E., 2006. Intersections of remanence small circles: new tools to improve data processing and interpretation in palaeomagnetism. Geophys. J. Int. 166, 33–45. doi:10.1111/j.1365-246X.2006.02898.x

Weinberger, R., Agnon, A., Ron, H., 1997. Paleomagnetic reconstruction of a diapir emplacement: a case study from Sedom diapir, the Dead Sea Rift. J. Geophys. Res. 102, 5173–5192.

Table 1. Remanent magnetization parameters of the ChRM. n/N: number of samples used to calculate the site-mean paleomagnetic direction / number of demagnetized samples. DipDir: Dip direction. BBC: before bedding correction. ATBC: after total bedding correction. BFD: best fit direction. BFD-Ref. angle: angle between the BFD and the calculated remagnetization direction.

SITE	Coordinates (WGS84)		Age	Bedding		Paleo-Bedding			BBC		Fisher parameters		ATBC		BFD		BFD-Ref. angular distance	Reference
	Longitude	Latitude		Dip Dir	Dip	Dip Dir	Dip	n/N	Dec	Inc	α95	k	Dec	Inc	Dec	Inc		
DP01	-5.665333	32.127467	Aal.-Baj.	355	71	175	8	8/8	194.8	62.5	6.4	75.5	342.4	44.4	343.8	36.2	9.6	Calvín et al., 2017b
DP02	-5.666252	32.128031	Aal.-Baj.	350	60	350	3	8/8	253.3	70.2	4.3	166.7	327.1	30.3	326.2	33.5	5.1	Calvín et al., 2017b
DP03	-5.666942	32.128857	Aal.-Baj.	001	25	181	5	7/8	314.7	60.3	5	144.4	333.1	40	335	35.2	2.4	Calvín et al., 2017b
DP04	-5.667967	32.129517	Baj.-Bath.	355	14	175	6	8/8	320.5	52.0	6.8	68.1	328	39.9	330.1	34.1	1.8	Calvín et al., 2017b
DP05	-5.587417	32.142367	Toar.-Aal.	293	87	293	79	8/8	325.0	45.1	5.6	99.2	319.9	-34.1	321.3	38	9.4	Calvín et al., 2017b
DP06	-5.588833	32.142842	Toar.-Aal.	303	59	303	46	8/8	328.0	48.4	6.6	70.4	319.4	-7.5	323.4	36.4	7.4	Calvín et al., 2017b
DP07	-5.590900	32.153424	Aal.-Baj.	325	70	325	8	8/8	090.7	79.2	1.6	1178.8	334.7	26	335.6	34.3	2.8	Calvín et al., 2017b
DP08	-5.590217	32.125674	Aal.-Baj.	138	82	138	74	7/8	345.1	24.6	8.7	48.8	83.9	59.3	347.2	31.8	12.8	Calvín et al., 2017b
DP09	-5.594883	32.125183	Aal.-Baj.	124	78	124	58	8/8	332.1	16.4	4.1	185.7	46.5	62.4	336.7	33.3	4	Calvín et al., 2017b
DP10	-5.598700	32.128833	Aal.-Baj.	333	71	333	74	7/8	321.9	31.2	5.7	115.1	320.8	-38.7	321.5	34	8.8	Calvín et al., 2017b
DP11	-5.601567	32.128941	Aal.-Baj.	305	51	305	51	8/8	323.4	36.1	3.7	219.5	320.2	-13	323.4	36.3	7.3	Calvín et al., 2017b
DP12	-5.588783	32.125612	Bath.	060	25	60	41	5/8	343.1	33.4	7.9	94.1	356.4	24.8	332.3	35.5	1	Calvín et al., 2017b
DP13	-5.600567	32.061133	Baj.	175	27	355	4	6/8	328.1	05.0	9.6	49.29	324.1	28.7	322.8	32.3	8.2	This work
DP14	-5.601109	32.058163	Baj.	333	58	333	49	7/8	346.6	42.4	6.6	84.4	343.3	-14.6	345.1	33.9	10.7	This work
IC04	-5.629883	32.161967	Bath.	348	22	348	11	8/8	336.4	46.6	12.2	21.6	335.3	23.8	333.8	34.7	1.3	Torres-López et al., 2014
IC46	-5.560222	32.135609	Bath.	324	49	324	4	7/8	31.6	65.8	19.1	10.9	349.6	28.7	350.5	31.9	15.5	Torres-López et al., 2014
IC47	-5.550108	32.118278	Bath.	342	85	342	70	8/8	31.6	65.8	13.2	18.6	327.1	-33.8	327.1	34	4.3	Torres-López et al., 2014
IC52	-5.476490	31.870688	Sinem.	313	10	313	11	7/8	344.7	31.3	24.3	7.1	342.1	22.7	344.9	31.7	11	Torres-López et al., 2014
IC53	-5.465222	31.856627	Sinem.	105	39	105	3	9/10	308.8	08.8	7.1	53.9	318.3	43.5	316.7	40.7	13.7	Torres-López et al., 2014
IC54	-5.468583	31.804349	Aal.-Baj.	154	11	334	6	8/7	331.9	17.5	13.7	20.3	331.7	28.5	331.6	34.5	0.5	Torres-López et al., 2014
ILA06	-5.609032	32.136854	Baj.	315	46	315	13	6/6	341.2	66.5	4.6	215.4	326	22.3	327.4	35.1	4	This work
ILA07	-5.608960	32.136928	Aal.-Baj.	308	25	308	15	5/6	347.8	39.2	6.3	148.7	339.6	18.7	343.6	31.5	10	This work
ILA08	-5.609935	32.138198	Aal.-Baj.	238	81	148	3	5/5	100.1	51.1	6.9	123.7	1.5	32.5	0.6	30.2	24.3	This work

ILA09	-5.616795	32.145754	Aal.-Baj.	326	44	326	7	5/6	304.6	70.2	15	27	318	27.2	317.4	34.4	12.2	This work
ILA20	-5.597218	31.945817	Baj.	158	19	158	26	5/7	334.8	42.0	5.4	153.5	333.1	61	335.1	34.6	2.4	This work
ILA21	-5.600967	31.952781	Baj.	148	56	148	57	6/7	337.5	35.2	15.2	20.3	69.4	82.1	337.4	34.2	4.3	This work
ILB06	-5.605602	32.029138	Baj.	339	45	159	26	7/8	174.2	73.6	7.6	64.5	330.3	60.6	333.8	34.6	1.4	This work
ILB11	-5.610734	31.972227	Baj.	164	28	344	12	4/8	323.5	-05.0	10.8	72.8	322	21.2	319.5	32.6	10.7	This work
ILB12	-5.613047	31.960845	Baj.	323	59	323	41	4/8	346.5	50.1	23.5	16.2	337.9	-6.3	340.9	33.6	7.3	This work
ILB13	-5.611863	31.959237	Baj.	340	60	340	65	5/8	342.4	29.5	9.5	65.3	342.4	-30.5	342.5	34.7	8.5	This work
SK03	-5.552833	32.123864	Bath.	339	75	339	48	7/8	352	61.4	7.9	49.6	345.3	-12.9	346.5	34.5	11.8	Calvín et al., 2017b
TM01	-5.520719	31.840945	Hett.	178	25	178	25	8/8	336.4	35.0	6.6	72.4	324	57.3	336.3	35.4	3.5	This work
TM02	-5.500862	31.845844	Hett.	180	38	180	22	8/8	334.2	20.1	4.5	149.5	318	52.3	330.4	34.1	1.5	This work
TM04	-5.489845	31.844744	Hett.	172	79	172	19	8/8	346.5	-23.9	3.9	204.98	343.3	54.7	345.8	36	11.2	This work
TM05	-5.480297	31.830942	Pliens.-Toar.	152	27	152	16	7/8	324.9	23.4	10.7	33.07	321.8	50.1	324.1	34.3	6.7	This work
TM06	-5.481719	31.835901	Hett.-Sinem.	182	12	2	11	5/6	312.9	10.8	15.3	20.2	310.5	18.5	307.5	24.7	23.5	This work
TM07	-5.481719	31.835901	Hett.-Sinem.	138	37	138	8	5/6	323.0	06.4	9.8	62.1	324.8	43.2	324.1	35.2	6.7	This work
TM08	-5.482122	31.840737	Hett.-Sin.	156	40	156	19	8/8	326.8	13.0	5.7	94.24	321.3	52.2	325.2	34.1	5.8	This work
TM09	-5.484549	31.843696	Hett.	158	50	158	19	5/8	336.4	03.8	4.4	300.77	335.3	53.8	336.1	34.6	3.2	This work
TM11	-5.511277	31.821042	Pliens.-Toar.	178	40	178	20	7/8	336.6	16.5	8.2	54.87	323.1	52.3	332.8	34.7	0.5	This work
TM12	-5.540931	31.813803	Pliens.-Toar.	158	30	158	3	4/8	332.7	07.4	11.2	68.66	331.4	37.2	331.6	34.5	0.5	This work
TM13	-5.470787	31.868641	Toar.-Aal.	314	78	314	14	5/8	061.2	60.2	17.5	20.16	344.1	18.9	347.7	31.1	13.4	This work
TM14	-5.470827	31.869095	Toar.-Aal.	146	12	326	5	6/8	340.1	16.8	4.1	272.55	341.4	28.4	342.3	33.6	8.4	This work
TM15	-5.470659	31.866227	Hett.	175	88	175	21	8/8	322.5	-26.6	5.7	95.6	309.6	47.6	320.6	31.6	10.1	This work
TM16	-5.479769	31.884229	Baj.-Aal.	007	65	-	-	0/8	-	-	-	-	-	-	-	-	-	This work
TM17	-5.505608	31.854215	Toar.-Aal.	304	47	304	23	7/8	345.2	54.7	10.3	35.48	327.1	13.8	331.6	34.7	0.5	This work
TM18	-5.505320	31.853987	Toar.-Aal.	304	75	304	38	7/8	005.5	60.4	6.5	87.66	329.7	-0.1	335.4	33.7	2.8	This work
TM19	-5.506541	31.855322	Toar.-Aal.	325	24	325	22	8/8	333.7	36.3	6.3	77.73	332.2	12.5	333.5	34.4	1.1	This work
TM20	-5.499786	31.856561	Toar.-Aal.	327	78	327	56	8/8	333.9	56.0	5.5	104.02	331.1	-21.8	331.7	34.5	0.4	This work

TM21	-5.497711	31.860331	Toar.-Aal.	337	60	337	36	7/8	330.2	58.6	5.3	150.58	333.5	-1.2	332.7	34.5	0.4	This work
TM22	-5.490631	31.865333	Toar.-Aal.	348	27	348	33	7/7	334.4	28.7	2	879.55	336.1	2.3	333.5	34.7	1.1	This work
TM23	-5.530925	31.844204	Toar.-Aal.	342	31	162	0	8/8	298.5	58.9	7.8	51.25	317	32.8	317.1	32.3	12.8	This work

Figure 1. (a) The Altlas Chain in the context of the Western Mediterranean framework. (b) Geological map of the Central High Altas (CHA) and location of the study area (Fig. 2). (c) Simplified temporal evolution of the main geological events occurred in the CHA. (a) and (b) modified after Teixell et al.(2003).

Figure 2. Geological map (a) and A-A' cross-section showing the four ridges analyzed in this work, as well as the paleomagnetic sites. A *.kml !le with the same information can be obtained in the supplementary material. The geological cartography is based in previous works (Heitzmann and Stüder, 1990; Hadri, 1997; Milhi, 1997; Fadile, 2003; Michard et al., 2011; Saura et al., 2014; Calvín et al., 2017).

Figure 3. Orthogonal plots of NRM of representative samples, plotted in in situ coordinates. (a) Typical signature of the samples, showing the component A with unblocking temperatures between 250 and 450ºC, going to the origin. (b) Presence of goethite. (c) In some samples, the component A does not go to the origin because of the presence of the high temperature (up to 500ºC) and high coercivity component B, which shows either normal and reverse polarities. (d) Samples with absence of component A. Calculated A and B component are in the supplemetary. (e) Hysteresis loops back!eld cycle and thermomagnetic curves of one representative sample. (f) Hysteresis parameters plot and mixing curves for magnetite (Dunlop, 2002) showing a mixture between SP and SSD in the measured samples.

Figure 4. (a-b) Bootstrap fold-test (Tauxe and Watson, 1994) of the components A and B using sample directions. Both components are interpreted as remagnetizations: component A can be clearly interpreted as a syn-folding remagnetization, whereas component B is almost post-folding. (a) Equal area projection of the site mean paleomagnetic directions of the ChRM (component A) and the corresponding small circles used to calculate the remagnetization direction. Mean directions of component A are in the Supplementary. BBC and ATBC: Before and after total tectonic correction respectively. BFD: Best !t direction. A/n matrix (Waldhör and Appel, 2006), calculated remagnetization direction (reference direction for restoration) and Kent's 95% con!dence ellipse (Calvín et al., 2017c).

Figure 5. Present-day (a) and ca. 100 Ma (b) B-B' cross-sections across the Ikkou ridge, showing the paleomagnetic sites used in the restoration. (c) Paleomagnetic directions with their respective small circles used in this work. (d) Chevron north-verging folds of the northern limb of the ridge. (e) Restoration of the northern limb of the Ikkou structure. SK03, IC46, IC47 and IC48 sites are extrapolated from the East.

Figure 6. Present-day (a) and ca. 100 Ma (b) C-C' cross-sections across the Tadaghmamt ridge and paleomagnetic sites used in the restoration. (c) Paleomagnetic directions with their respective small circles used in this work. (d) Core of the ridge showing the large amount of Triassic basalts, capped by Bajocian limestones. (e) Picture taken towards the W showing the core of the ridge, with Triassic red-shales capped by Bajocian limestones. (f) Core of the Ridge and fold in its southern limb.

Figure 7. Present-day (a) and ca. 100 Ma (b) D-D' cross-sections across the Timedouine ridge showing the paleomagnetic sites used in the restoration. (c) Paleomagnetic directions with their respective small circles used in this work. (d) Easternmost end of the Timedouine ridge, showing Triassic red-shales and Jurassic gabbros in the core, and Bajocian limestones as the overburden. (e) Local sedimentary unconformities in the Aalenian-Bajocian marls.

Figure 8. Present-day (a) and ca. 100 Ma (b) E-E' cross-sections across the Toumliline ridge showing the paleomagnetic sites used in the restoration. (c) Paleomagnetic directions with their respective small circles used in this work. (d) The Toumliline diapir, showing Triassic shales and basalts in its core, and the Hettangian in its southern limb thrusting over the Aalenian-Bajocian in its northern limb. (e) Present-day and ca. 100 Ma F-F' cross-section showing that most part of the present-day deformation is related to Cenozoic thrusting.

Figure 9. Present-day and ca. 100 Ma cross sections along the study area. The cross-section is composed by the B-B', C-C', D-D' AND E-E' cross-sections.

Highlights

Pre-compression restoration of salt-related structures in the Central High Atlas

Differentiation between extensional salt-walls and upright thrust anticlines

Widespread ca. 100 Ma remagnetization affecting Jurassic carbonates

Use of remagnetization to restore paleo-attitude of the beds in sedimentary basins